Available online at www.sciencedirect.com
ScienceDirect
Comput. Methods Appl. Mech. Engrg. 196 (2007) 1203–1215
Computer methods in applied mechanics and engineering
www.elsevier.com/locate/cma

Non-linear strain–displacement equations exactly representing large rigid-body motions. Part III. Analysis of TM shells with constraints

G.M. Kulikov *, S.V. Plotnikova

Department of Applied Mathematics and Mechanics, Tambov State Technical University, 106 Sovetskaya Street, Tambov 392000, Russia

Received 31 October 2005; received in revised form 20 April 2006; accepted 29 August 2006

Abstract

The precise representation of arbitrarily large rigid-body motions in the displacement patterns of curved Timoshenko–Mindlin-type (TM) shell elements has been considered in Part I of the present work. In Part II it has been developed an enhanced mixed finite element formulation that allows using load increments that are much larger than possible with existing geometrically exact displacement-based shell element formulations. In this paper the developed formulation is employed to solve frictionless contact problems for TM shells undergoing finite deformations and interacting with rigid bodies. The contact conditions are incorporated into the assumed stress–strain TM shell formulation by applying a perturbed Lagrangian procedure with the fundamental unknowns consisting of 6 displacements and 11 strains of the bottom and top surfaces of the shell, 11 conjugate stress resultants and the Lagrange multiplier, associated with a nodal contact force, through using the non-conventional technique. The efficiency and accuracy of the proposed finite element formulation are demonstrated by means of several numerical examples.

Keywords: Geometrically exact solid-shell element; Finite deformation; Unilateral constraints; Perturbed Lagrangian formulation

1. Introduction

The considerable progress has been achieved in recent years on the development of finite element procedures for the geometrically non-linear shells with constraints [1–7] in conjunction with the perturbed Lagrangian formulation, which was originally proposed in papers [8,9]. This methodology is discussed in detail in books [10,11]. However, an implementation of such procedures to shells undergoing finite deformations and contacting with rigid bodies of *arbitrary* configurations may lead to inefficient computations because only small loading steps are available. This is due to the simple fact that contact pressure is equal exactly to the value of the Lagrange multiplier.

In the present paper it is developed the new non-linear geometrically exact shell model with unilateral constraint conditions, based on the enhanced finite element technique, that a nodal contact force normal to the constraint surface is associated with the Lagrange multiplier λ as $\lambda|\mathrm{grad}\,\Psi|$, where Ψ is the impenetrability function. This allows one to use much larger load increments by employing non-linear geometrically exact TM shell elements [12,13]. It is worth noting that in the case of the successful choice of the initial contact zone a solution of the contact problem can be obtained, as a rule, in *one loading step* for the extremely large displacements and rotations, i.e., only the trial-and-error procedure will work in conjunction with the Newton iteration process of course.

The direct use of the conventional first-order TM shell theory (see in this context a discussion in Refs. [12,14])

* Corresponding author. Fax: +7 475 253 2017.
E-mail addresses: kulikov@apmath.tstu.ru, gmkulikov@mail.ru (G.M. Kulikov).
URL: http://apm.tstu.ru/kulikov (G.M. Kulikov).

0045-7825/$ - see front matter © 2006 Elsevier B.V. All rights reserved.
doi:10.1016/j.cma.2006.08.016

for solving contact problems is not always convenient. In such problems it is more convenient to select as unknown functions the displacements of the bottom and top surfaces of the shell, since by means of these displacements the kinematic requirement of no penetration of the contact bodies is formulated. To overcome shear and membrane locking and have no spurious zero energy modes, the assumed strain and stress resultant fields are invoked. So, additional fundamental unknowns have to be involved in the formulation, namely, 11 strains of the outer surfaces and 11 conjugate stress resultants [12,14]. In order to circumvent thickness locking, the ad hoc modified constitutive stiffness matrix [15–18] corresponding to the general plane stress state is employed.

Numerical results are presented to demonstrate the high accuracy and effectiveness of the finite element formulation developed and to compare its performance with other state-of-the-art finite element formulations. For this purpose three tests are employed. They are a plate in cylindrical bending, a circular ring and a cylindrical shell in contact with a rigid infinite cylinder.

2. Contact formulation for 3D shell

Consider a shell of the thickness h interacting with a rigid body (Fig. 1). The shell may be defined as a 3D body of volume V bounded by two surfaces S^- and S^+, located at the distances δ^- and δ^+ measured with respect to the reference surface S, and the edge boundary surface Ω that is perpendicular to the reference surface. The shell material is assumed to be linearly elastic, anisotropic, homogeneous or fiber reinforced, such that in each point there is a single surface of elastic symmetry parallel to the reference surface.

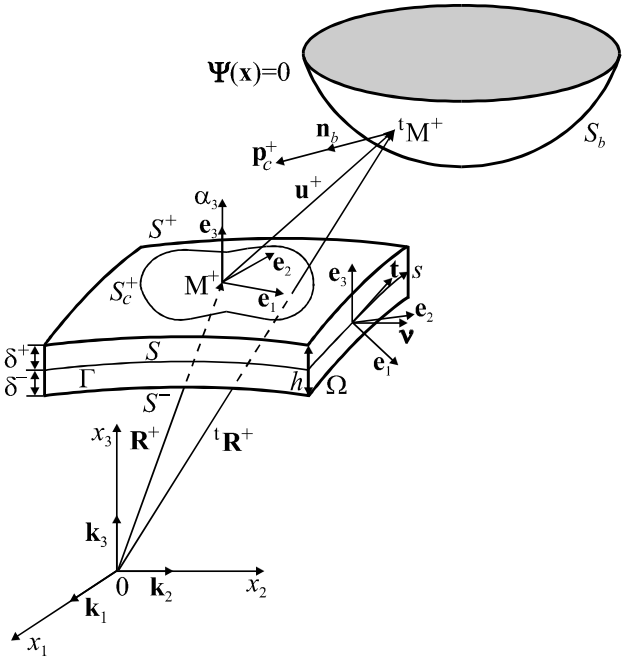

Fig. 1. Shell in contact with rigid body.

Introduce the following notations: u_i are the components of the displacement vector; S_{ij} are the components of the second Piola–Kirchhoff stress tensor; $\varepsilon_{ij}^{\mathrm{DS}}$ are the components of the Green–Lagrange strain tensor (we refer to these strains as displacement-dependent strains); $\varepsilon_{ij}^{\mathrm{AS}}$ are the components of the independently assumed strain tensor (displacement-independent strains); $C_{ij\ell m}$ are the components of the elasticity tensor. Throughout this paper the abbreviation $(\,)_{,i}$ implies the partial derivatives with respect to the coordinate x_i; indices i, j, ℓ, m take the values 1, 2 and 3, while Greek indices α, β, γ, δ take the values 1 and 2.

For general purposes we can treat the interaction between a shell and many rigid bodies, but for the simplicity we restrict ourselves to the frictionless contact problem and one rigid body. The boundary of the immovable convex body S_{b} is supposed to be sufficiently smooth and may be written as

$$\Psi(\mathbf{x}) = 0, \tag{1a}$$

where $\mathbf{x} = x_i\mathbf{k}_i$ is the position vector of the surface S_{b}. Here, in accordance with the Einstein convention the summation on the repeated index is implied. We shall follow this rule in the following developments.

For the external points of the rigid body it is assumed that

$$\Psi(\mathbf{x}) > 0. \tag{1b}$$

We treat Eqs. (1a) and (1b) as the impenetrability condition for the shell and rigid body. These equations express the fact that when two bodies are in contact, then they must either remain in contact according to Eq. (1a) or they must separate in accordance with Eq. (1b). The impenetrability condition (1) is highly non-linear for the finite deformation shell problems but in our formulation may be usually expressed *analytically* in terms of displacements of the top surface S^+ and, therefore, is simply linearized. The surface S^+ consists of two distinct parts $S^+ = S_{\mathrm{f}}^+ \cup S_{\mathrm{c}}^+$, where S_{f}^+ is the part where surface tractions are prescribed and S_{c}^+ is the part where a contact interaction is expected, whereas the bottom surface $S^- = S_{\mathrm{f}}^-$. So, no prescribed displacements are imposed on both face surfaces.

Taking into account that no adhesion between the contact surfaces in the normal direction may occur, the normal contact tractions cannot be tensile

$$p_{\mathrm{c}}^+ = -\mathbf{p}_{\mathrm{c}}^+ \cdot \mathbf{n}_{\mathrm{b}} \leqslant 0, \tag{2}$$

where $\mathbf{n}_{\mathrm{b}}$ is the unit normal vector to the body surface S_{b}.

Conditions (1) and (2) may be combined into a single equation

$$p_{\mathrm{c}}^+(\mathbf{R}^+)\Psi({}^t\mathbf{R}^+) = 0, \tag{3a}$$

$${}^t\mathbf{R}^+ = \mathbf{R}^+ + \mathbf{u}^+, \quad \mathbf{u}^+ = u_i^+\mathbf{k}_i, \tag{3b}$$

where $\mathbf{R}^+$ and ${}^t\mathbf{R}^+$ are the position vectors of the top surface S^+ in initial and current shell configurations; $\mathbf{u}^+$ is the displacement vector of the surface S^+. The condition (3) is called the unitary contact condition and expresses

the fact that the contact forces exist only at points, where the shell is in contact with the rigid body.

For the simplicity, we limit our discussion to the case of zero body forces and dead loading. Furthermore, all prescribed displacements on the edge boundary surface Ω_d are assumed to be zero. To arrive at the assumed stress–strain shell formulation without contact constraints, we should invoke the stationarity of the Hu–Washizu functional [19]

$$J_{HW} = \text{stationary}, \tag{4a}$$

$$J_{HW} = \int\int\int_V \left[\frac{1}{2}\varepsilon_{ij}^{AS} C_{ij\ell m}\varepsilon_{\ell m}^{AS} - S_{ij}(\varepsilon_{ij}^{AS} - \varepsilon_{ij}^{DS})\right] dV - \int\int_\Sigma p_i u_i \, dS - \int\int_{\Omega_d} \sigma_i u_i \, dS, \tag{4b}$$

where

$$\varepsilon_{ij}^{DS} = \frac{1}{2}(u_{i,j} + u_{j,i} + u_{k,i}u_{k,j}). \tag{5}$$

Here, p_i are the tractions applied to the surface $\Sigma = S^- \cup S_f^+ \cup \Omega_f$; σ_i are the unknown tractions over the edge boundary surface Ω_d defined as

$$\sigma_i = S_{kj} v_j (\delta_{ik} + u_{i,k}), \tag{6}$$

where v_j are the components of the unit normal vector $\boldsymbol{\nu}$.

In order to introduce the contact constraints (1) into a variational formulation, we consider the modified Hu–Washizu functional (one refers to it as a perturbed Lagrangian [8])

$$J_{PL} = \text{stationary}, \tag{7a}$$

$$J_{PL} = J_{HW} + \int\int_{S_c^+} \left[\lambda \Psi({}^t\mathbf{R}^+) - \frac{\lambda^2}{2\epsilon}\right] dS, \tag{7b}$$

where $\lambda(\mathbf{R}^+)$ is the Lagrange multiplier; ϵ is the positive penalty parameter. The penalty term serves the purpose of the regularization of the classical Lagrangian and amounts to approximating the rigid body by continuously distributed springs of the stiffness $1/\epsilon$. Note that in the limit $\epsilon \to \infty$ one arrives at the pure Lagrangian formulation [20].

By invoking the stationarity of the functional J_{PL} with respect to the independent variables, we obtain

$$\int\int\int_V [\delta\varepsilon_{ij}^{AS}(S_{ij} - C_{ij\ell m}\varepsilon_{\ell m}^{AS}) + \delta S_{ij}(\varepsilon_{ij}^{AS} - \varepsilon_{ij}^{DS})]\, dV - \int\int\int_V S_{ij}\delta\varepsilon_{ij}^{DS}\, dV + \int\int_\Sigma p_i \delta u_i \, dS + \int\int_{\Omega_d} (\delta\sigma_i u_i + \sigma_i \delta u_i)\, dS - \int\int_{S_c^+} \left[\lambda\delta\Psi({}^t\mathbf{R}^+) + \delta\lambda\left(\Psi({}^t\mathbf{R}^+) - \frac{1}{\epsilon}\lambda\right)\right] dS = 0. \tag{8}$$

Next we prove a fundamental result concerning the relation between normal contact tractions and a Lagrange multiplier.

Proposition 1. *The following closed-form expression for the normal contact force holds*:

$$p_c^+ = \lambda(\mathbf{R}^+)|\operatorname{grad}\Psi({}^t\mathbf{R}^+)|. \tag{9}$$

Proof. Substituting strains (5) into the second 3D integral (8) and applying Gauss' theorem with account for relations (2) and (6), one derives

$$\mathbf{p}_c^+ \cdot \delta\mathbf{u}^+ = -\lambda\delta\Psi({}^t\mathbf{R}^+). \tag{10}$$

By using Eq. (3b) a variation of the impenetrability function can be represented as

$$\delta\Psi({}^t\mathbf{R}^+) = \operatorname{grad}\Psi({}^t\mathbf{R}^+)\cdot\delta\mathbf{u}^+. \tag{11}$$

Comparing Eqs. (10) and (11) yields

$$\mathbf{p}_c^+ = -\lambda \operatorname{grad}\Psi({}^t\mathbf{R}^+). \tag{12}$$

The required formula (9) immediately follows from Eqs. (2) and (12). □

It should be observed that Eq. (9) allows one to use much larger load increments compared to conventional shell formulations under unilateral constraints.

3. Contact formulation for TM shell

Let the reference surface S be referred to the orthogonal curvilinear coordinate system α_1 and α_2, which coincides with the lines of principal curvatures of its surface, whereas the coordinate α_3 is oriented along the unit vector e_3 normal to the reference surface; $\mathbf{e}_\alpha$ are the tangent unit vectors to the lines of principal curvatures (Fig. 1); A_α are the Lamé coefficients of the reference surface.

The finite deformation TM shell theory [13] is based on the linear approximation of displacements in the thickness direction (Timoshenko–Mindlin kinematics)

$${}^t\mathbf{R} = N^-{}^t\mathbf{R}^- + N^+{}^t\mathbf{R}^+, \tag{13a}$$

$${}^t\mathbf{R}^\pm = \mathbf{R}^\pm + \mathbf{v}^\pm, \quad \mathbf{R}^\pm = \mathbf{r} + \delta^\pm\mathbf{e}_3, \tag{13b}$$

$$\mathbf{v}^\pm = v_i^\pm \mathbf{e}_i, \tag{13c}$$

$$N^- = \frac{1}{h}(\delta^+ - \alpha_3), \quad N^+ = \frac{1}{h}(\alpha_3 - \delta^-), \tag{13d}$$

where $\mathbf{r}(\alpha_1, \alpha_2)$ is the position vector of the reference surface; $\mathbf{R}^\pm$ and ${}^t\mathbf{R}^\pm$ are the position vectors of the face surfaces $S^\pm$ in initial and current shell configurations; $\mathbf{v}^\pm$ are the displacement vectors of the face surfaces; $v_i^\pm(\alpha_1, \alpha_2)$ are the components of these vectors, which are always measured in accordance with the total Lagrangian formulation from the initial configuration to the current configuration directly; $N^\pm(\alpha_3)$ are the linear through-thickness shape functions. It is remarkable that displacement vectors (13c) are resolved in the orthonormal reference surface basis $\mathbf{e}_i$ that allows one to reduce the costly numerical integration by deriving the elemental stiffness matrix.

We represent further the impenetrability condition (1) in curvilinear reference surface coordinates. Let the Cartesian

coordinate frame be defined by the unit base vectors $\mathbf{k}_i$ (Fig. 1). The needed vectors in this frame are given by

$$\mathbf{r} = r_i\mathbf{k}_i, \quad {}^t\mathbf{R}^+ = {}^tR_i^+\mathbf{k}_i, \quad \mathbf{e}_i = t_{ij}\mathbf{k}_j, \tag{14}$$

where $\mathbf{T} = [t_{ij}(\alpha_1, \alpha_2)]$ is the transformation matrix. Using Eqs. (13b), (13c) and (14) one derives

$${}^tR_i^+ = r_i + \delta^+ t_{3i} + t_{ji}v_j^+. \tag{15}$$

So, the kinematic condition of no penetration and a variation of the impenetrability function (11) may be written as

$$\Psi(\alpha_1, \alpha_2, v_i^+) \geqslant 0, \tag{16}$$

$$\delta\Psi = \frac{\partial\Psi}{\partial v_i^+}\delta v_i^+. \tag{17}$$

Substituting displacements (13), displacement-dependent and displacement-independent strains [13] and a variation of the impenetrability function (17) into variational equation (8), and introducing stress resultants and external loading resultants

$$H_{\alpha\beta}^{\pm} = \int_{\delta^-}^{\delta^+} S_{\alpha\beta}N^{\pm}\,\mathrm{d}\alpha_3, \quad H_{\alpha 3}^{\pm} = \int_{\delta^-}^{\delta^+} S_{\alpha 3}N^{\pm}\,\mathrm{d}\alpha_3,$$

$$H_{33} = \int_{\delta^-}^{\delta^+} S_{33}\,\mathrm{d}\alpha_3, \quad \widehat{H}_{v\text{æ}}^{\pm} = \int_{\delta^-}^{\delta^+} q_{\text{æ}}N^{\pm}\,\mathrm{d}\alpha_3$$

$$(\text{æ} = v, t \text{ and } 3), \tag{18}$$

one can obtain the mixed variational equation for the TM shell element under unilateral constraints

$$\int\int_{S^{\mathrm{el}}} [\delta\mathbf{E}^{\mathrm{T}}(\mathbf{H} - \mathbf{D}\mathbf{E}) + \delta\mathbf{H}^{\mathrm{T}}(\mathbf{E} - \boldsymbol{\mathscr{E}}) - \delta\boldsymbol{\mathscr{E}}^{\mathrm{T}}\mathbf{H} + \delta\mathbf{v}^{\mathrm{T}}\mathbf{P}]\bar{\mu}\,\mathrm{d}\xi_1\,\mathrm{d}\xi_2$$

$$- \delta J_{\mathrm{c}} + \oint_{\Gamma^{\mathrm{el}}} \delta\mathbf{v}_{\Gamma}^{\mathrm{T}}\widehat{\mathbf{H}}_{\Gamma}\bar{\gamma}\,\mathrm{d}s = 0, \tag{19a}$$

$$\delta J_{\mathrm{c}} = \int\int_{S_{\mathrm{c}}^{\mathrm{el}}} \delta g\,\mathrm{d}\xi_1\,\mathrm{d}\xi_2, \quad \delta g = \bar{\mu}\left[\delta\mathbf{v}^{\mathrm{T}}\lambda\boldsymbol{\Phi} + \delta\lambda\left(\Psi - \frac{1}{\epsilon}\lambda\right)\right]. \tag{19b}$$

In relations (19) the following notations are introduced:

$$\mathbf{v} = [v_1^- \; v_1^+ \; v_2^- \; v_2^+ \; v_3^- \; v_3^+]^{\mathrm{T}}, \quad \mathbf{v}_{\Gamma} = [v_v^- \; v_v^+ \; v_t^- \; v_t^+ \; v_3^- \; v_3^+]^{\mathrm{T}},$$

$$\boldsymbol{\mathscr{E}} = [\mathscr{E}_{11}^- \; \mathscr{E}_{11}^+ \; \mathscr{E}_{22}^- \; \mathscr{E}_{22}^+ \; 2\mathscr{E}_{12}^- \; 2\mathscr{E}_{12}^+ \; 2\mathscr{E}_{13}^- \; 2\mathscr{E}_{13}^+ \; 2\mathscr{E}_{23}^- \; 2\mathscr{E}_{23}^+ \; \mathscr{E}_{33}]^{\mathrm{T}},$$

$$\mathbf{E} = [E_{11}^- \; E_{11}^+ \; E_{22}^- \; E_{22}^+ \; 2E_{12}^- \; 2E_{12}^+ \; 2E_{13}^- \; 2E_{13}^+ \; 2E_{23}^- \; 2E_{23}^+ \; E_{33}]^{\mathrm{T}},$$

$$\mathbf{H} = [H_{11}^- \; H_{11}^+ \; H_{22}^- \; H_{22}^+ \; H_{12}^- \; H_{12}^+ \; H_{13}^- \; H_{13}^+ \; H_{23}^- \; H_{23}^+ \; H_{33}]^{\mathrm{T}},$$

$$\widehat{\mathbf{H}}_{\Gamma} = [\widehat{H}_{vv}^- \; \widehat{H}_{vv}^+ \; \widehat{H}_{vt}^- \; \widehat{H}_{vt}^+ \; \widehat{H}_{v3}^- \; \widehat{H}_{v3}^+]^{\mathrm{T}},$$

$$\mathbf{P} = [-p_1^- \; p_1^+ \; -p_2^- \; p_2^+ \; -p_3^- \; p_3^+]^{\mathrm{T}},$$

$$\boldsymbol{\Phi} = \left[0 \; \frac{\partial\Psi}{\partial v_1^+} \; 0 \; \frac{\partial\Psi}{\partial v_2^+} \; 0 \; \frac{\partial\Psi}{\partial v_3^+}\right]^{\mathrm{T}}, \quad \bar{\mu} = \overline{A}_1^{\mathrm{el}}\overline{A}_2^{\mathrm{el}},$$

$$\bar{\gamma} = 1 + k_{\mathrm{N}}\bar{\delta}, \quad \bar{\delta} = \frac{1}{2}(\delta^- + \delta^+), \tag{20}$$

where $\overline{A}_{\alpha}^{\mathrm{el}} = A_{\alpha}\ell_{\alpha}^{\mathrm{el}}(1 + k_{\alpha}\bar{\delta})$ are the Lamé coefficients of the midsurface $\overline{S}^{\mathrm{el}}$ of the element (no summation is used); $\xi_{\gamma} = (\alpha_{\gamma} - d_{\gamma}^{\mathrm{el}})/\ell_{\gamma}^{\mathrm{el}}$ are the curvilinear normalized coordinates (Fig. 2); $d_{\gamma}^{\mathrm{el}} = (\alpha_{\gamma}^{-\mathrm{el}} + \alpha_{\gamma}^{+\mathrm{el}})/2$ are the coordinates of the center of the element; $2\ell_{\gamma}^{\mathrm{el}} = \alpha_{\gamma}^{+\mathrm{el}} - \alpha_{\gamma}^{-\mathrm{el}}$ are the lengths of the element; k_{α} are the principal curvatures of the reference surface S^{el} of the element; k_{N} is the normal curvature of the bounding curve $\Gamma^{\mathrm{el}} \subset S^{\mathrm{el}}$; $\bar{\delta}$ is the distance from the reference surface to the midsurface; $v_v^{\pm}, v_t^{\pm}$ and $v_3^{\pm}$ are the components of the displacement vectors of the face surfaces in the coordinate system v, t and α_3 (Fig. 1); q_v, q_t and q_3 are the tractions applied to the edge boundary surface $\Omega^{\mathrm{el}} = \Omega_{\mathrm{f}}^{\mathrm{el}}$; $p_i^{\pm}$ are the tractions acting on the face surfaces $S^{\pm\mathrm{el}}$; $\mathscr{E}_{\alpha\beta}^{\pm}, \mathscr{E}_{\alpha 3}^{\pm}$ and $\mathscr{E}_{33}$ are the components of the Green–Lagrange strain tensor of the face surfaces [13]; $E_{\alpha\beta}^{\pm}, E_{\alpha 3}^{\pm}$ and E_{33} are the components of the independently assumed strain tensor of the face surfaces; $\mathbf{D}$ is the constitutive stiffness matrix defined in Refs. [13,17].

Remark 1. The integrals in variational equation (8) have been simplified under the following assumption: the metrics of all surfaces parallel to the reference surface are identical and equal to the metric of the midsurface. It is a reasonable assumption for the thin-walled shell structures.

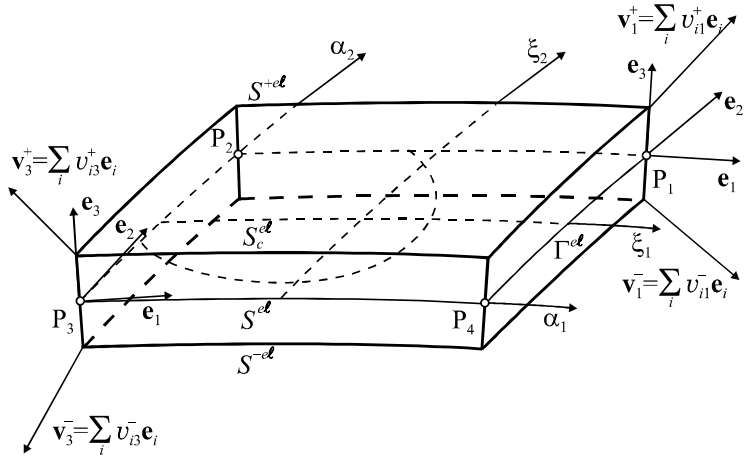

Fig. 2. Four-node TM shell element. $P_1(\alpha_1^{+\mathrm{el}}, \alpha_2^{+\mathrm{el}}), P_2(\alpha_1^{-\mathrm{el}}, \alpha_2^{+\mathrm{el}}), P_3(\alpha_1^{-\mathrm{el}}, \alpha_2^{-\mathrm{el}}), P_4(\alpha_1^{+\mathrm{el}}, \alpha_2^{-\mathrm{el}})$ are the nodal points of the element.

Remark 2. To circumvent thickness locking, the more robust remedy compared to Refs. [12,13] has been employed. This remedy consists of using the *ad hoc* modified constitutive stiffness matrix $\mathbf{D}^{\mathrm{PS}}$, corresponding to the generalized plane-stress condition [15–18], instead of the matrix $\mathbf{D}$ in variational equation (19). The advantage of such approach is that the simplified constitutive stiffness matrix possesses the symmetric structure, which is best suited for the finite element application to contact problems (see for detail [17]).

4. Finite element formulation

For the simplest four-node *curved* solid-shell element the displacement field is approximated according to the standard C^0 interpolation

$$\mathbf{v} = \sum_r N_r \mathbf{v}_r, \tag{21}$$

where $\mathbf{v}_r = [v_{1r}^- \; v_{1r}^+ \; v_{2r}^- \; v_{2r}^+ \; v_{3r}^- \; v_{3r}^+]^{\mathrm{T}}$ are the displacement vectors of the element nodes; $N_r(\xi_1,\xi_2)$ are the bilinear shape functions of the element; the subscript r denotes a number of nodes and runs from 1 to 4. The load vector is also assumed to vary bilinearly inside the element.

In a result for the displacement-dependent strains we have the following approximation [13]:

$$\boldsymbol{\mathscr{E}} = \sum_{s_1,s_2} \xi_1^{s_1}\xi_2^{s_2}\boldsymbol{\mathscr{E}}^{s_1s_2}, \tag{22a}$$

$$\begin{aligned}
&\boldsymbol{\mathscr{E}}^{s_1s_2} = (\mathbf{B}^{s_1s_2} + \mathbf{A}^{s_1s_2}\mathbf{V})\mathbf{V}, \quad \mathbf{B}^{s_1s_2} = \mathbf{0} \text{ for } s_1 = 2 \text{ or } s_2 = 2,\\
&\boldsymbol{\mathscr{E}}^{s_1s_2} = [\mathscr{E}_{11}^{-s_1s_2} \; \mathscr{E}_{11}^{+s_1s_2} \; \mathscr{E}_{22}^{-s_1s_2} \; \mathscr{E}_{22}^{+s_1s_2} \; 2\mathscr{E}_{12}^{-s_1s_2} \; 2\mathscr{E}_{12}^{+s_1s_2}\\
&\qquad 2\mathscr{E}_{13}^{-s_1s_2} \; 2\mathscr{E}_{13}^{+s_1s_2} \; 2\mathscr{E}_{23}^{-s_1s_2} \; 2\mathscr{E}_{23}^{+s_1s_2} \; \mathscr{E}_{33}^{s_1s_2}]^{\mathrm{T}},
\end{aligned} \tag{22b}$$

where $\mathbf{V} = [\mathbf{v}_1^{\mathrm{T}} \; \mathbf{v}_2^{\mathrm{T}} \; \mathbf{v}_3^{\mathrm{T}} \; \mathbf{v}_4^{\mathrm{T}}]^{\mathrm{T}}$ is the displacement vector at nodal points of the element; $\mathbf{B}^{s_1s_2}$ are the matrices of order 11×24 corresponding to the linear strain–displacement transformation; $\mathbf{A}^{s_1s_2}$ are the 3D arrays of order $11\times 24\times 24$ corresponding to the non-linear strain–displacement transformation, involved in the formulation to simplify the matrix routine; $\mathbf{A}^{s_1s_2}\mathbf{V}$ are the matrices of order 11×24 and $\mathbf{HA}^{s_1s_2}$ are the symmetric matrices of order 24×24, whose components are defined as

$$\begin{aligned}
&(\mathbf{A}^{s_1s_2}\mathbf{V})_{n_1n_2} = \sum_{n_3} A^{s_1s_2}_{n_1n_2n_3}V_{n_3}, \quad (\mathbf{HA}^{s_1s_2})_{n_2n_3} = \sum_{n_1} H_{n_1}A^{s_1s_2}_{n_1n_2n_3},\\
&A^{s_1s_2}_{n_1n_2n_3} = A^{s_1s_2}_{n_1n_3n_2} \qquad (\text{for } n_1 = \overline{1,11} \text{ and } n_2,n_3 = \overline{1,24}).
\end{aligned} \tag{23}$$

Throughout this section superscripts s_1, s_2 take the values 0, 1 and 2. From Eq. (23) follows the noteworthy transformation

$$(\mathbf{A}^{s_1s_2}\mathbf{V})^{\mathrm{T}}\mathbf{H} = (\mathbf{HA}^{s_1s_2})\mathbf{V} \tag{24}$$

to be used for evaluating the element stiffness matrix.

Note that the described non-linear four-node curved solid-shell element a bit stiff in a case of using coarse meshes and some additional numerical procedure needs to be applied. The best solution of the problem is to employ the modified ANS method [13]. The main idea of such approach can be traced back to the ANS method proposed by Hughes and Tezduyar [21] for the linear displacement-based formulation and further developed by many scientists for the linear and non-linear displacement, hybrid and mixed finite element formulations. In contrast with above formulations we treat the term ANS formulation in the broad sense. In our formulation all components of the displacement-dependent strain tensor are assumed to vary bilinearly inside the element [13] instead of the expected biquadratic interpolation (22a) typical for the non-linear four-node solid-shell elements, that is,

$$\begin{aligned}
\boldsymbol{\mathscr{E}}^{\mathrm{ANS}} = {}& \boldsymbol{\mathscr{E}}^{00} + \boldsymbol{\mathscr{E}}^{02} + \boldsymbol{\mathscr{E}}^{20} + \boldsymbol{\mathscr{E}}^{22} + \xi_1(\boldsymbol{\mathscr{E}}^{10} + \boldsymbol{\mathscr{E}}^{12})\\
&+ \xi_2(\boldsymbol{\mathscr{E}}^{01} + \boldsymbol{\mathscr{E}}^{21}) + \xi_1\xi_2\boldsymbol{\mathscr{E}}^{11}.
\end{aligned} \tag{25}$$

For evaluating the integral (19b) it is convenient to employ the simplest numerical scheme

$$\delta J_{\mathrm{c}} = \sum_r \delta g_r = \sum_r \bar{\mu}_r \left[\delta\mathbf{v}_r^{\mathrm{T}}\lambda_r\boldsymbol{\Phi}_r + \delta\lambda_r\left(\Psi_r - \frac{1}{\epsilon}\lambda_r\right)\right], \tag{26}$$

where

$$\begin{aligned}
&\boldsymbol{\Phi}_r = \left[0 \; \frac{\partial\Psi_r}{\partial v_{1r}^+} \; 0 \; \frac{\partial\Psi_r}{\partial v_{2r}^+} \; 0 \; \frac{\partial\Psi_r}{\partial v_{3r}^+}\right]^{\mathrm{T}}, \quad \frac{\partial\Psi_r}{\partial v_{ir}^+} = \frac{\partial\Psi}{\partial v_i^+}(P_r),\\
&\Psi_r = \Psi(P_r).
\end{aligned} \tag{27}$$

This is due to the bilinear interpolation of the function δg from Eq. (19b):

$$\delta g = \sum_r N_r \delta g_r, \tag{28}$$

where δg_r are the nodal values of this function. The proposed scheme gives an opportunity to eliminate nodal Lagrange parameters λ_r at the element level and leads to the governing system of linear algebraic equations with the symmetric stiffness matrix.

Remark 3. In Refs. [6,7], in contrast with the developed TM shell formulation with unilateral constraints, the Lagrange multiplier λ has been approximated according to the bilinear law. As a result, the nodal Lagrange parameters λ_r are not eliminated on the local level and difficulties, associated with the equation system whose size varies during the solution process, can occur.

To avoid shear and membrane locking and have no spurious zero energy modes, the assumed strain and stress resultant fields inside the element [12] are introduced

$$\mathbf{E}=\sum_{r_1,r_2}\xi_1^{r_1}\xi_2^{r_2}\mathbf{Q}^{r_1r_2}\mathbf{E}^{r_1r_2},\quad \mathbf{H}=\sum_{r_1,r_2}\xi_1^{r_1}\xi_2^{r_2}\mathbf{Q}^{r_1r_2}\mathbf{H}^{r_1r_2},\tag{29}$$

$$\begin{aligned}
&\mathbf{E}^{00}=[E_{11}^{-00}\ E_{11}^{+00}\ E_{22}^{-00}\ E_{22}^{+00}\ 2E_{12}^{-00}\ 2E_{12}^{+00}\ 2E_{13}^{-00}\ 2E_{13}^{+00}\ 2E_{23}^{-00}\ 2E_{23}^{+00}\ E_{33}^{00}]^{\mathrm{T}},\\
&\mathbf{E}^{01}=[E_{11}^{-01}\ E_{11}^{+01}\ 2E_{13}^{-01}\ 2E_{13}^{+01}\ E_{33}^{01}]^{\mathrm{T}},\\
&\mathbf{E}^{10}=[E_{22}^{-10}\ E_{22}^{+10}\ 2E_{23}^{-10}\ 2E_{23}^{+10}\ E_{33}^{10}]^{\mathrm{T}},\quad \mathbf{E}^{11}=[E_{33}^{11}],\\
&\mathbf{H}^{00}=[H_{11}^{-00}\ H_{11}^{+00}\ H_{22}^{-00}\ H_{22}^{+00}\ H_{12}^{-00}\ H_{12}^{+00}\ H_{13}^{-00}\ H_{13}^{+00}\ H_{23}^{-00}\ H_{23}^{+00}\ H_{33}^{00}]^{\mathrm{T}},\\
&\mathbf{H}^{01}=[H_{11}^{-01}\ H_{11}^{+01}\ H_{13}^{-01}\ H_{13}^{+01}\ H_{33}^{01}]^{\mathrm{T}},\\
&\mathbf{H}^{10}=[H_{22}^{-10}\ H_{22}^{+10}\ H_{23}^{-10}\ H_{23}^{+10}\ H_{33}^{10}]^{\mathrm{T}},\quad \mathbf{H}^{11}=[H_{33}^{11}],
\end{aligned}\tag{30}$$

where $\mathbf{Q}^{00}$ is the identity matrix of order 11×11; $\mathbf{Q}^{01}$ and $\mathbf{Q}^{10}$ are the matrices from zeros and units of order 11×5, and $\mathbf{Q}^{11}$ is the matrix of order 11×1 defined in Ref. [12]. Throughout this section superscripts r_1, r_2 take the values 0 and 1.

Substituting approximations (21), (25), (26) and (29) into mixed variational equation (19a) and using a standard variational procedure, one obtains the governing system of non-linear algebraic equations of the developed finite element formulation

$$\mathbf{E}^{r_1r_2}=(\mathbf{Q}^{r_1r_2})^{\mathrm{T}}(\mathbf{B}^{r_1r_2}+\mathbf{R}^{r_1r_2}\mathbf{V})\mathbf{V},\tag{30a}$$

$$\mathbf{H}^{r_1r_2}=(\mathbf{Q}^{r_1r_2})^{\mathrm{T}}\mathbf{D}\mathbf{Q}^{r_1r_2}\mathbf{E}^{r_1r_2},\tag{30b}$$

$$\sum_{r_1,r_2}\frac{1}{3^{r_1+r_2}}(\mathbf{B}^{r_1r_2}+2\mathbf{R}^{r_1r_2}\mathbf{V})^{\mathrm{T}}\mathbf{Q}^{r_1r_2}\mathbf{H}^{r_1r_2}+\boldsymbol{\Xi}\boldsymbol{\Lambda}=\mathbf{F},\tag{30c}$$

where $\mathbf{F}$ is the force vector corresponding to the standard displacement-based formulation; $\boldsymbol{\Lambda}$ is the Lagrange multiplier vector at nodal points; $\mathbf{R}^{r_1r_2}$ are the 3D arrays of order $11\times 24\times 24$ defined as

$$\begin{aligned}
&\mathbf{R}^{00}=\mathbf{A}^{00}+\mathbf{A}^{02}+\mathbf{A}^{20}+\mathbf{A}^{22},\quad \mathbf{R}^{01}=\mathbf{A}^{01}+\mathbf{A}^{21},\\
&\mathbf{R}^{10}=\mathbf{A}^{10}+\mathbf{A}^{12},\quad \mathbf{R}^{11}=\mathbf{A}^{11},\quad \boldsymbol{\Lambda}=[\lambda_1\lambda_2\lambda_3\lambda_4]^{\mathrm{T}},\\
&\boldsymbol{\Xi}=\tfrac{1}{4}\begin{bmatrix}\boldsymbol{\Phi}_1 & \mathbf{O}_{6\times1} & \mathbf{O}_{6\times1} & \mathbf{O}_{6\times1}\\ \mathbf{O}_{6\times1} & \boldsymbol{\Phi}_2 & \mathbf{O}_{6\times1} & \mathbf{O}_{6\times1}\\ \mathbf{O}_{6\times1} & \mathbf{O}_{6\times1} & \boldsymbol{\Phi}_3 & \mathbf{O}_{6\times1}\\ \mathbf{O}_{6\times1} & \mathbf{O}_{6\times1} & \mathbf{O}_{6\times1} & \boldsymbol{\Phi}_4\end{bmatrix}.
\end{aligned}\tag{31}$$

Additionally, according to Eqs. (3a), (12) and (26) the following relations need to be involved into the finite element formulation:

$$\Psi_r=\frac{1}{\epsilon}\lambda_r,\quad \lambda_r\leqslant 0\qquad \text{for } r\in I_{\mathrm{C}},\tag{32a}$$

$$\Psi_r>0,\quad \lambda_r=0\qquad \text{for } r\notin I_{\mathrm{C}},\tag{32b}$$

where $I_{\mathrm{C}}\subset\{1,2,3,4\}$ denotes a set of contacting nodes.

Up to this moment, no incremental arguments are needed in the total Lagrangian formulation. These arguments are required for solving non-linear equilibrium equations (30) with constraints (32) on the basis of the Newton–Raphson method. Further, the left superscripts t and $t+\Delta t$ indicate in which configuration at time t or time $t+\Delta t$ a quantity occurs. Then, in accordance with this agreement we have

$$\begin{aligned}
&{}^{t+\Delta t}\mathbf{V}={}^{t}\mathbf{V}+\Delta\mathbf{V},\quad {}^{t+\Delta t}\mathbf{F}={}^{t}\mathbf{F}+\Delta\mathbf{F},\quad {}^{t+\Delta t}\boldsymbol{\Lambda}={}^{t}\boldsymbol{\Lambda}+\Delta\boldsymbol{\Lambda},\\
&{}^{t+\Delta t}\mathbf{E}^{r_1r_2}={}^{t}\mathbf{E}^{r_1r_2}+\Delta\mathbf{E}^{r_1r_2},\quad {}^{t+\Delta t}\mathbf{H}^{r_1r_2}={}^{t}\mathbf{H}^{r_1r_2}+\Delta\mathbf{H}^{r_1r_2}.
\end{aligned}\tag{33}$$

Substituting (33) in Eq. (30) and taking into account that the external loads and second Piola–Kirchhoff stresses constitute the self-equilibrated system in a configuration at time t, one can obtain the following incremental equations:

$$\Delta\mathbf{E}^{r_1r_2}=(\mathbf{Q}^{r_1r_2})^{\mathrm{T}}({}^{t}\mathbf{M}^{r_1r_2}+\mathbf{R}^{r_1r_2}\Delta\mathbf{V})\Delta\mathbf{V},\tag{34a}$$

$$\Delta\mathbf{H}^{r_1r_2}=\overline{\mathbf{D}}^{r_1r_2}\Delta\mathbf{E}^{r_1r_2},\tag{34b}$$

$$\begin{aligned}
&\sum_{r_1,r_2}\frac{1}{3^{r_1+r_2}}[2(\mathbf{R}^{r_1r_2}\Delta\mathbf{V})^{\mathrm{T}}\mathbf{Q}^{r_1r_2}{}^{t}\mathbf{H}^{r_1r_2}+({}^{t}\mathbf{M}^{r_1r_2}+2\mathbf{R}^{r_1r_2}\Delta\mathbf{V})^{\mathrm{T}}\mathbf{Q}^{r_1r_2}\Delta\mathbf{H}^{r_1r_2}]\\
&\quad+\boldsymbol{\Xi}|_{{}^{t+\Delta t}\mathbf{V}}{}^{t+\Delta t}\boldsymbol{\Lambda}=\Delta\mathbf{F}+\boldsymbol{\Xi}|_{{}^{t}\mathbf{V}}{}^{t}\boldsymbol{\Lambda},
\end{aligned}\tag{34c}$$

where

$$\begin{aligned}
&\mathbf{D}^{r_1r_2}=\mathbf{Q}^{r_1r_2}\overline{\mathbf{D}}^{r_1r_2}(\mathbf{Q}^{r_1r_2})^{\mathrm{T}},\quad \overline{\mathbf{D}}^{r_1r_2}=(\mathbf{Q}^{r_1r_2})^{\mathrm{T}}\mathbf{D}\mathbf{Q}^{r_1r_2},\\
&{}^{t}\mathbf{M}^{r_1r_2}=\mathbf{B}^{r_1r_2}+2\mathbf{R}^{r_1r_2}{}^{t}\mathbf{V}.
\end{aligned}\tag{35}$$

From relations (32) one finds

$$\Psi_r|_{{}^{t+\Delta t}\mathbf{V}}=\frac{1}{\epsilon}{}^{t+\Delta t}\lambda_r,\quad {}^{t+\Delta t}\lambda_r\leqslant 0\qquad \text{for } r\in {}^{t+\Delta t}I_{\mathrm{C}},\tag{36a}$$

$$\Psi_r|_{{}^{t+\Delta t}\mathbf{V}}>0,\quad {}^{t+\Delta t}\lambda_r=0\qquad \text{for } r\notin {}^{t+\Delta t}I_{\mathrm{C}}\tag{36b}$$

and, therefore,

$${}^{t+\Delta t}\lambda_r=\begin{cases}\epsilon\Psi_r|_{{}^{t+\Delta t}\mathbf{V}} & \text{for } r\in {}^{t+\Delta t}I_{\mathrm{C}},\\ 0 & \text{for } r\notin {}^{t+\Delta t}I_{\mathrm{C}},\end{cases}\tag{37}$$

where ${}^{t+\Delta t}I_{\mathrm{C}}$ is the set of unknown a priori contact nodes at time $t+\Delta t$.

Using (37) we eliminate nodal Lagrange parameters ${}^{t+\Delta t}\lambda_r$ from Eq. (34c)

$$\begin{aligned}
&\sum_{r_1,r_2}\frac{1}{3^{r_1+r_2}}[2(\mathbf{R}^{r_1r_2}\Delta\mathbf{V})^{\mathrm{T}}\mathbf{Q}^{r_1r_2}{}^{t}\mathbf{H}^{r_1r_2}\\
&\quad+({}^{t}\mathbf{M}^{r_1r_2}+2\mathbf{R}^{r_1r_2}\Delta\mathbf{V})^{\mathrm{T}}\mathbf{Q}^{r_1r_2}\Delta\mathbf{H}^{r_1r_2}]+\epsilon(\boldsymbol{\Xi}\boldsymbol{\Pi})|_{{}^{t+\Delta t}\mathbf{V}}\\
&\quad=\Delta\mathbf{F}+\boldsymbol{\Xi}|_{{}^{t}\mathbf{V}}{}^{t}\boldsymbol{\Lambda},
\end{aligned}\tag{38}$$

where

$$\boldsymbol{\Pi}=[\Pi_1\ \Pi_2\ \Pi_3\ \Pi_4]^{\mathrm{T}},\tag{39a}$$

$$\Pi_r=\begin{cases}\Psi_r & \text{for } r\in {}^{t+\Delta t}I_{\mathrm{C}},\\ 0 & \text{for } r\notin {}^{t+\Delta t}I_{\mathrm{C}}.\end{cases}\tag{39b}$$

Due to existence of non-linear terms in Eqs. (34) and (38), the Newton–Raphson iteration process should be employed

$$\begin{aligned}
&\Delta\mathbf{V}^{[n+1]}=\Delta\mathbf{V}^{[n]}+\Delta\mathscr{V}^{[n]},\quad \Delta\mathbf{E}^{r_1r_2[n+1]}=\Delta\mathbf{E}^{r_1r_2[n]}+\Delta\mathbf{E}^{r_1r_2[n]},\\
&\Delta\mathbf{H}^{r_1r_2[n+1]}=\Delta\mathbf{H}^{r_1r_2[n]}+\Delta\mathscr{H}^{r_1r_2[n]}\qquad (n=0,1,\ldots)
\end{aligned}\tag{40}$$

to solve these equations

$$\Delta\mathbf{E}^{r_1r_2[n]} - (\mathbf{Q}^{r_1r_2})^{\mathrm{T}}\,{}^{t}\mathbf{L}^{r_1r_2[n]}\Delta\boldsymbol{\mathscr{V}}^{[n]} = (\mathbf{Q}^{r_1r_2})^{\mathrm{T}}({}^{t}\mathbf{L}^{r_1r_2[n]} - \mathbf{R}^{r_1r_2}\Delta\mathbf{V}^{[n]})\Delta\mathbf{V}^{[n]} - \Delta\mathbf{E}^{r_1r_2[n]}, \tag{41a}$$

$$\Delta\boldsymbol{\mathscr{H}}^{r_1r_2[n]} - \overline{\mathbf{D}}^{r_1r_2}\Delta\mathbf{E}^{r_1r_2[n]} = \overline{\mathbf{D}}^{r_1r_2}\Delta\mathbf{E}^{r_1r_2[n]} - \Delta\mathbf{H}^{r_1r_2[n]}, \tag{41b}$$

$$\begin{aligned}\sum_{r_1,r_2}\frac{1}{3^{r_1+r_2}}&[2(\mathbf{R}^{r_1r_2}\Delta\boldsymbol{\mathscr{V}}^{[n]})^{\mathrm{T}}\mathbf{Q}^{r_1r_2}({}^{t}\mathbf{H}^{r_1r_2} + \Delta\mathbf{H}^{r_1r_2[n]})\\ &+ ({}^{t}\mathbf{L}^{r_1r_2[n]})^{\mathrm{T}}\mathbf{Q}^{r_1r_2}\Delta\boldsymbol{\mathscr{H}}^{r_1r_2[n]}] + \epsilon\mathbf{K}_{\mathrm{C}}\Delta\boldsymbol{\mathscr{V}}^{[n]}\\ &= \Delta\mathbf{F} - \sum_{r_1,r_2}\frac{1}{3^{r_1+r_2}}[2(\mathbf{R}^{r_1r_2}\Delta\mathbf{V}^{[n]})^{\mathrm{T}}\mathbf{Q}^{r_1r_2}\,{}^{t}\mathbf{H}^{r_1r_2}\\ &\quad + ({}^{t}\mathbf{L}^{r_1r_2[n]})^{\mathrm{T}}\mathbf{Q}^{r_1r_2}\Delta\mathbf{H}^{r_1r_2[n]}] - \epsilon(\boldsymbol{\Xi}\boldsymbol{\Pi})|_{{}^{t}\mathbf{V}+\Delta\mathbf{V}^{[n]}} + \boldsymbol{\Xi}|_{{}^{t}\mathbf{V}}\,{}^{t}\boldsymbol{\Lambda},\end{aligned} \tag{41c}$$

where

$${}^{t}\mathbf{L}^{r_1r_2[n]} = \mathbf{B}^{r_1r_2} + 2\mathbf{R}^{r_1r_2}({}^{t}\mathbf{V} + \Delta\mathbf{V}^{[n]}) = {}^{t}\mathbf{M}^{r_1r_2} + 2\mathbf{R}^{r_1r_2}\Delta\mathbf{V}^{[n]}, \tag{42a}$$

$$\mathbf{K}_{\mathrm{C}} = \begin{bmatrix} \boldsymbol{\mathfrak{a}}_1 & \mathbf{O}_{6\times6} & \mathbf{O}_{6\times6} & \mathbf{O}_{6\times6} \\ \mathbf{O}_{6\times6} & \boldsymbol{\mathfrak{a}}_2 & \mathbf{O}_{6\times6} & \mathbf{O}_{6\times6} \\ \mathbf{O}_{6\times6} & \mathbf{O}_{6\times6} & \boldsymbol{\mathfrak{a}}_3 & \mathbf{O}_{6\times6} \\ \mathbf{O}_{6\times6} & \mathbf{O}_{6\times6} & \mathbf{O}_{6\times6} & \boldsymbol{\mathfrak{a}}_4 \end{bmatrix}, \tag{42b}$$

where $\boldsymbol{\mathfrak{a}}_r$ are the matrices of order 6×6 defined as

$$\boldsymbol{\mathfrak{a}}_r = \mathbf{O}_{6\times6} \quad \text{for } r \notin {}^{t+\Delta t}I_{\mathrm{C}}. \tag{43a}$$

The non-zero components of the remaining matrices are found by

$$(\boldsymbol{\mathfrak{a}}_r)_{2i,2j} = \left(\Psi_r\frac{\partial^2\Psi_r}{\partial v_{ir}^{+}\partial v_{jr}^{+}} + \frac{\partial\Psi_r}{\partial v_{ir}^{+}}\frac{\partial\Psi_r}{\partial v_{jr}^{+}}\right)|_{{}^{t}\mathbf{V}+\Delta\mathbf{V}^{[n]}} \quad \text{for } r \in {}^{t+\Delta t}I_{\mathrm{C}}. \tag{43b}$$

Eliminating further incremental strains $\Delta\mathbf{E}^{r_1r_2[n]}$ and stress resultants $\Delta\boldsymbol{\mathscr{H}}^{r_1r_2[n]}$ from Eq. (41) and taking into account the transformation (24), one derives linear algebraic equations

$$\mathbf{K}\Delta\boldsymbol{\mathscr{V}}^{[n]} = \Delta\boldsymbol{\mathscr{F}}^{[n]}, \tag{44}$$

where

$$\begin{aligned}\Delta\boldsymbol{\mathscr{F}}^{[n]} = \Delta\mathbf{F} - \sum_{r_1,r_2}\frac{1}{3^{r_1+r_2}}&[({}^{t}\mathbf{L}^{r_1r_2[n]})^{\mathrm{T}}\mathbf{D}^{r_1r_2}({}^{t}\mathbf{L}^{r_1r_2[n]} - \mathbf{R}^{r_1r_2}\Delta\mathbf{V}^{[n]})\\ &+ 2(\mathbf{Q}^{r_1r_2}\,{}^{t}\mathbf{H}^{r_1r_2})\mathbf{R}^{r_1r_2}]\Delta\mathbf{V}^{[n]} - \epsilon(\boldsymbol{\Xi}\boldsymbol{\Pi})|_{{}^{t}\mathbf{V}+\Delta\mathbf{V}^{[n]}} + \boldsymbol{\Xi}|_{{}^{t}\mathbf{V}}\,{}^{t}\boldsymbol{\Lambda}.\end{aligned} \tag{45}$$

As usual in the finite element literature $\mathbf{K} = \mathbf{K}_D + \mathbf{K}_H + \epsilon\mathbf{K}_{\mathrm{C}}$ denotes the elemental stiffness matrix defined by Eq. (42b) and

$$\mathbf{K}_D = \sum_{r_1,r_2}\frac{1}{3^{r_1+r_2}}({}^{t}\mathbf{L}^{r_1r_2[n]})^{\mathrm{T}}\mathbf{D}^{r_1r_2}\,{}^{t}\mathbf{L}^{r_1r_2[n]}, \tag{46a}$$

$$\mathbf{K}_H = 2\sum_{r_1,r_2}\frac{1}{3^{r_1+r_2}}(\mathbf{Q}^{r_1r_2}\,{}^{t}\mathbf{H}^{r_1r_2} + \mathbf{Q}^{r_1r_2}\Delta\mathbf{H}^{r_1r_2[n]})\mathbf{R}^{r_1r_2}. \tag{46b}$$

We give also a formula that is used in the numerical algorithm for computation of incremental stress resultants at the nth iteration step

$$\begin{aligned}\mathbf{Q}^{r_1r_2}\Delta\mathbf{H}^{r_1r_2[n]} = \mathbf{D}^{r_1r_2}&[({}^{t}\mathbf{M}^{r_1r_2} + 2\mathbf{R}^{r_1r_2}\Delta\mathbf{V}^{[n-1]})\Delta\mathbf{V}^{[n]}\\ &- (\mathbf{R}^{r_1r_2}\Delta\mathbf{V}^{[n-1]})\Delta\mathbf{V}^{[n-1]}].\end{aligned} \tag{47}$$

This formula holds for $n \geqslant 1$ while at the beginning of the first iteration one should set

$$\Delta\mathbf{V}^{[0]} = \mathbf{0} \quad \text{and} \quad \Delta\mathbf{H}^{r_1r_2[0]} = \mathbf{0}. \tag{48}$$

Allowing for relations (42), (45)–(48) the equilibrium equation (44) for each element are assembled by the usual technique to form the global incremental equilibrium equations. These incremental equations should be performed until the required accuracy of the solution can be obtained. The convergence criterion used here can be described as

$$\|\mathbf{r}^{[n]}\| < \varepsilon\|\mathbf{r}^{[0]}\|, \tag{49}$$

where $\mathbf{r}^{[n]}$ is the residual; $\|\cdot\|$ is the Euclidean norm; ε is the prescribed tolerance.

It is apparent that the contact non-linearity arises already during the finite element discretization. This is due to the fact that a set of all contact nodes after the assembly procedure ${}^{t+\Delta t}I_{\mathrm{C}}^{\mathrm{A}} \subset \{1,2,\ldots,N^{\mathrm{node}}\}$ is unknown a priori. To solve this problem, a trial-and-error procedure [10] has to be employed at each load step. Suppose that all contact nodes at time $t+\Delta t$ are known and, therefore, one can find a solution of the governing equations iteratively satisfying the convergence criteria (49). Since the global displacement vector ${}^{t+\Delta t}\mathbf{U}$ is known, we may verify inequalities

$$\Psi_L|_{{}^{t+\Delta t}\mathbf{U}} > 0 \quad \text{for } L \in {}^{t+\Delta t}I_{\mathrm{C}}^{\mathrm{A}}, \tag{50a}$$

$$\Psi_L|_{{}^{t+\Delta t}\mathbf{U}} \leqslant 0 \quad \text{for } L \notin {}^{t+\Delta t}I_{\mathrm{C}}^{\mathrm{A}}. \tag{50b}$$

If (50a) holds then such node is the error node and it is discarded. In the case of the fulfilment of (50b) a node is involved into a set ${}^{t+\Delta t}I_{\mathrm{C}}^{\mathrm{A}}$. This process is repeated until a correct solution without error nodes can be found.

5. Numerical examples

The performance of the developed geometrically exact assumed stress–strain solid-shell element TMS4HC is evaluated with several benchmark problems extracted from the literature and authors' examples as well. These problems are a plate in cylindrical bending, a circular ring and a cylindrical shell, which contact with movable and immovable rigid cylinders.

Unless specified otherwise, in all numerical problems the tolerance error from criterion (49) is set to be $\varepsilon = 10^{-10}$. Besides, in this section we use the following abbreviations: NLSt is a number of load steps employed to equally divide the maximum load; NTESt is a total number of trial-and-error steps needed for all loading increments; NNEt is a total number of Newton iterations.

5.1. Cylindrical bending of plate in contact with rigid cylinder

Consider first cylindrical bending of the isotropic plate contacting with movable (problem A) and immovable (problem B) rigid cylinders of the sufficiently large radius $R_b = 1000$. The geometrical and mechanical data of the contact problem are shown in Fig. 3. Due to symmetry of both problems, only half of the plate is discretized by the 100×1 mesh of TMS4HC elements. To solve problem A, the following boundary conditions have been used:

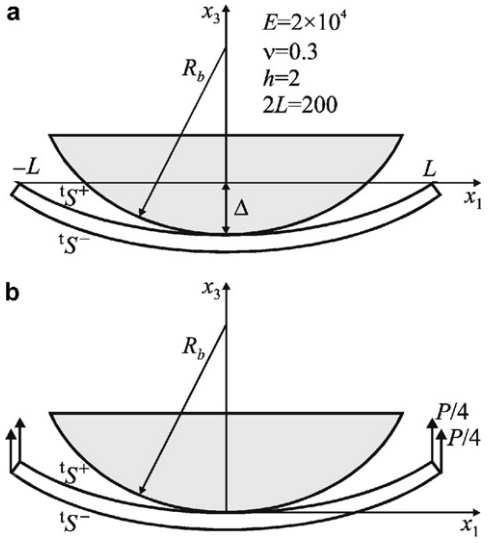

Fig. 3. Cylindrical bending of isotropic plate in contact with rigid cylinder: (a) Problem A (movable cylinder) and (b) Problem B (immovable cylinder).

$$v_1^{\pm}(0) = 0 \quad \text{and} \quad v_3^{+}(L) = 0. \tag{51}$$

The input data for each problem were taken from the analytical solution [22] derived for the geometrically linear plate interacting with a movable cylinder through the assumption that a contact zone is known and equal to $[0, 15]$. In a result there were found the cylinder displacement Δ and contact pressure resultant

$$P_c = 2\int_0^L \lambda \, dx_1, \tag{52a}$$

whose value of 0.3403 was used as an input value for problem B. At the same time for the calculation of the contact pressure resultant in the geometrically non-linear case we have employed the more general formula

$$P_c = 2\int_0^L \lambda \frac{\partial \Psi}{\partial v_3^+} \, dx_1. \tag{52b}$$

The impenetrability condition for the geometrically non-linear plate has been taken in a form

$$\Psi = \frac{1}{2R_b}(x_1 + v_1^+)^2 + \frac{1}{2R_b}(v_3^+ - R_b + \Delta)^2 - \frac{1}{2}R_b \geqslant 0. \tag{53}$$

Tables 1 and 2 list the results of solving both geometrically linear and non-linear contact problems. It should be mentioned that contact pressure [22] does not vanish at the end of the contact zone. This contradiction can be easily explained, since no regularization terms were introduced in contact conditions under analytical developments.

Further we consider a finite deformation problem for the plate contacting with the immovable cylinder of the small radius $R_b = 100$. Due to symmetry, one half of the

Table 1
Displacements and forces of plate in contact with rigid cylinder of radius $R_b = 1000$ (modeled by 100×1 mesh and penalty parameter $\epsilon = 10^5$)

Parameter	Linear plate		Non-linear plate		Analytical solution for problem A [22]
	Problem A	Problem B	Problem A	Problem B	
Δ	3.765[a]	0.0	3.765	0.0	3.765
$v_3^+(L)$	0.0	3.765	0.0	3.759	0.0
P		0.3403		0.3403	
P_c	0.3403	0.3403	0.3405	0.3404	0.3403

[a] Underlined numbers are input data for each problem.

Table 2
Distribution of contact pressure $p_c^+ L/P^{anal}$ for plate interacting with rigid cylinder of radius $R_b = 1000$ (modeled by 100×1 mesh and penalty parameter $\epsilon = 10^5$), where $P^{anal} = 0.3403$ [22]

x_1	Linear plate		Non-linear plate		Analytical solution for problem A [22]
	Problem A	Problem B	Problem A	Problem B	
10	0.019	0.022	0.003	0.036	0.223
11	0.954	0.964	0.789	0.943	0.920
12	3.639	3.669	3.139	3.605	3.099
13	10.21	10.28	9.113	10.13	8.839
14	20.06	20.13	18.90	19.97	20.68
15	15.11	14.94	18.06	15.31	33.25

Table 3
Convergence study for non-linear plate (Problem B) in contact with rigid cylinder of radius $R_b = 100$ by using 50×1 mesh

P	*Trial* contact zone	Penalty parameter ϵ	NLSt	NTESt	NNEt	Actual contact zone	$\bar{v}_3(L)$
2	{0}	10^3	1	1	4	{0}	21.65
2	{0}	10^5	1	1	8	{0}	21.65
4	{0}	10^3	1	21	85	$[0,4] \cup [16,20]$	36.73
4	{0}	10^5	1	22	108	$[0,10] \cup [16,20]$	36.73
6	{0}	10^3	2	34	122	$[0,30] \cup [38,42]$	41.26
6	{0}	10^5	3	46	160	$[0,34] \cup [38,42]$	41.26
6	[0, 50]	10^3	1	7	28	$[0,30] \cup [38,42]$	41.26
6	[0, 50]	10^5	1	9	58	$[0,34] \cup [38,42]$	41.26
8	{0}	10^3	3	53	191	$[0,44] \cup [50,54]$	42.98
8	{0}	10^5	4	60	200	[0,54]	42.98
8	[0, 50]	10^3	1	8	44	$[0,44] \cup [50,54]$	42.98
8	[0, 50]	10^5	2	46	204	[0, 54]	42.98

plate is modeled with the uniform 50×1 mesh of TMS4HC elements. Table 3 lists the convergence study, where $\bar{v}_3$ denotes the transverse midplane displacement. One can see that in the case of the successful choice of the trial contact zone only *one loading step* is needed to find a plate response for the extremely large rotations and displacements. Let us pay attention to the sufficiently large number of Newton iterations for $\epsilon = 10^5$ because large values of the penalty parameter lead to ill-conditioning of the governing system of equations. The effect of the magnitude of the penalty parameter ϵ on the accuracy of the contact pressure distribution over a deformed top surface is displayed in Figs. 4 and 5. As can be seen from Fig. 4, the distribution of contact pressure is highly sensitive to a choice of the penalty parameter. Additionally, the variation of the contact region with loading is shown in Fig. 6. As it turned out in the range of the loading parameter $P = 4$–12 there are two contact zones exactly.

5.2. Circular ring in contact with rigid cylinder

A circular isotropic ring pressed down against a rigid plate by a transverse force P at the apex was used as a benchmark problem for numerical testing the geometrically non-linear structures with unilateral constraints in Refs. [3,6,23]. But we study the more general case of contact constraints as shown in Fig. 7. The impenetrability conditions can be represented as

$$\Psi = {}^tR_3 \geqslant 0,$$
$$ {}^tR_3 = \left(R + \frac{1}{2}h\right)(1 - \cos\alpha_1) + v_1^+ \sin\alpha_1 - v_3^+ \cos\alpha_1 \tag{54a}$$

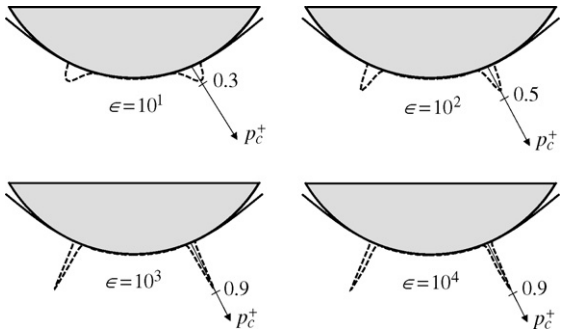

Fig. 4. Distribution of contact pressure over deformed top plate surface ${}^tS^+$ for $R_b = 100$ and $P = 6$ (modeled by 50×1 mesh).

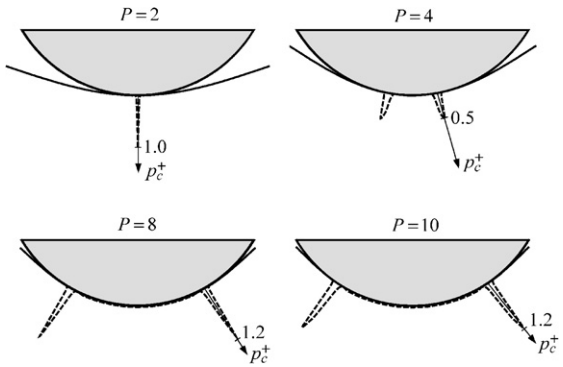

Fig. 5. Distribution of contact pressure over deformed top plate surface ${}^tS^+$ for $R_b = 100$ and $\epsilon = 10^3$ (modeled by 50×1 mesh).

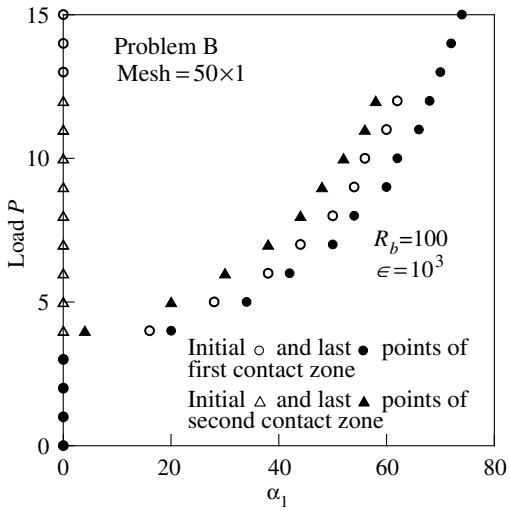

Fig. 6. Plate in contact with rigid cylinder. Variation of contact region with loading.

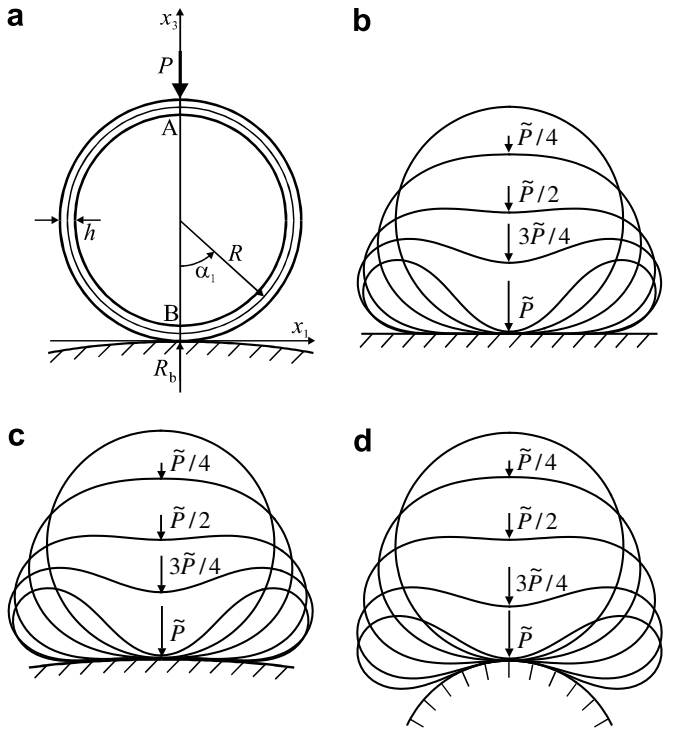

Fig. 7. Circular ring in contact with rigid cylinder: (a) geometry $E = 10^4$, $\nu = 0$, $R = 100$, $b = 1$, $h = 1$) and deformed configurations (modeled by 60×1 mesh) for (b) $R_b = \infty$, $\widetilde{P} = 88.4$, $\epsilon = 10^4$, (c) $R_b = 1000$, $\widetilde{P} = 88.5$, $\epsilon = 10^4$, and (d) $R_b = 100$, $\widetilde{P} = 83.2$, $\epsilon = 10^2$.

for a rigid plate, when $R_b = \infty$, and

$$\Psi = \frac{1}{2R_b}({}^tR_1)^2 + \frac{1}{2R_b}({}^tR_3 + R_b)^2 - \frac{1}{2}R_b \geqslant 0,$$
$$ {}^tR_1 = \left(R + \frac{1}{2}h\right)\sin\alpha_1 + v_1^+\cos\alpha_1 + v_3^+\sin\alpha_1 \tag{54b}$$

for a rigid cylinder of the radius R_b.

Owing to symmetry of the problem, only one half of the ring is discretized by regular 30×1 and 60×1 meshes of TMS4HC elements. It has been discovered that the deformation of the ring is inextensional in all ranges of the parameter R_b because the total strain energy is practically equal to the bending energy. Table 4 lists the convergence results for the ring and rigid cylinder of the radius $R_b = 1000$, which can be obtained again by using only one load step. It is seen that a value of 88.61 computed

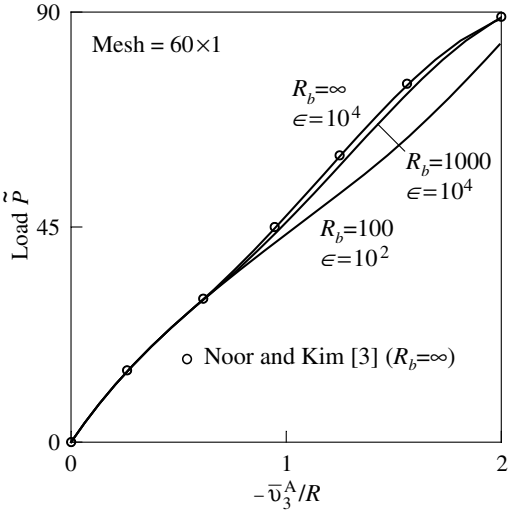

Fig. 8. Circular ring in contact with rigid cylinder. Top load versus transverse displacement of midcircle at section A.

for the dimensionless contact pressure resultant $\widetilde{P}_c = 120P_cR^2/Eh^3b$ employing the fine mesh, where

$$P_c = 2bR\int_0^\pi \lambda\left(-\frac{\partial\Psi}{\partial v_1^+}\sin\alpha_1 + \frac{\partial\Psi}{\partial v_3^+}\cos\alpha_1\right)\mathrm{d}\alpha_1, \tag{55}$$

agrees closely with an exact value of 88.50 of the dimensionless pinched load $\widetilde{P} = 120PR^2/Eh^3b$. Fig. 8 displays load–displacement curves for all considered cases of contact constraints and a comparison with results of Noor and Kim [3], where $\bar{v}_3^A$ denotes the transverse midcircle displacement at the top section A. For the complete picture Fig. 9 shows the variation of the contact region with loading. One can see that only a small part of the outer circle of the ring remains in contact, especially for the cylinder of the large curvature. This cannot be observed in Fig. 7 because gaps between bodies are very small.

5.3. Cylindrical shell in contact with rigid infinite cylinder

Finally, we consider a cylindrical shell subjected to the conservative concentrated load at its central section and interacting with a rigid plate and infinite cylinders of large and small radii. The first problem was earlier investigated in Ref. [6], where it is reported that the deformation of

Table 4
Convergence study for circular ring subjected to dimensionless load $\widetilde{P} = 88.5$ and interacting with rigid cylinder of radius $R_b = 1000$, where $\varphi_0 = \pi/60$, $d_1 = [10\varphi_0, 12\varphi_0]$ and $d_2 = [11\varphi_0, 12\varphi_0]$

Trial contact zone	Mesh	Penalty parameter ϵ	NLSt	NTESt	NNEt	Actual contact region	$\widetilde{P}_c$	$-\bar{v}_3^A$
$\{0\}$[a]	30×1	10^0	2	23	117	$\{0\} \cup d_1$	88.95	198.3
$\{0\}$[a]	30×1	10^4	5	31	152	$\{0\} \cup d_1$	88.95	198.3
$\{0\}$[a]	60×1	10^0	2	31	163	$[0, \varphi_0] \cup d_1$	88.61	198.8
$\{0\}$[a]	60×1	10^4	5	57	210	$[0, \varphi_0] \cup d_2$	88.61	198.8
$\{0\} \cup d_1$	30×1	10^0	1	1	8	$\{0\} \cup d_1$	88.95	198.3
$\{0\} \cup d_1$	60×1	10^0	1	3	24	$[0, \varphi_0] \cup d_1$	88.61	198.8

[a] Tolerance error is set to be $\varepsilon = 10^{-8}$.

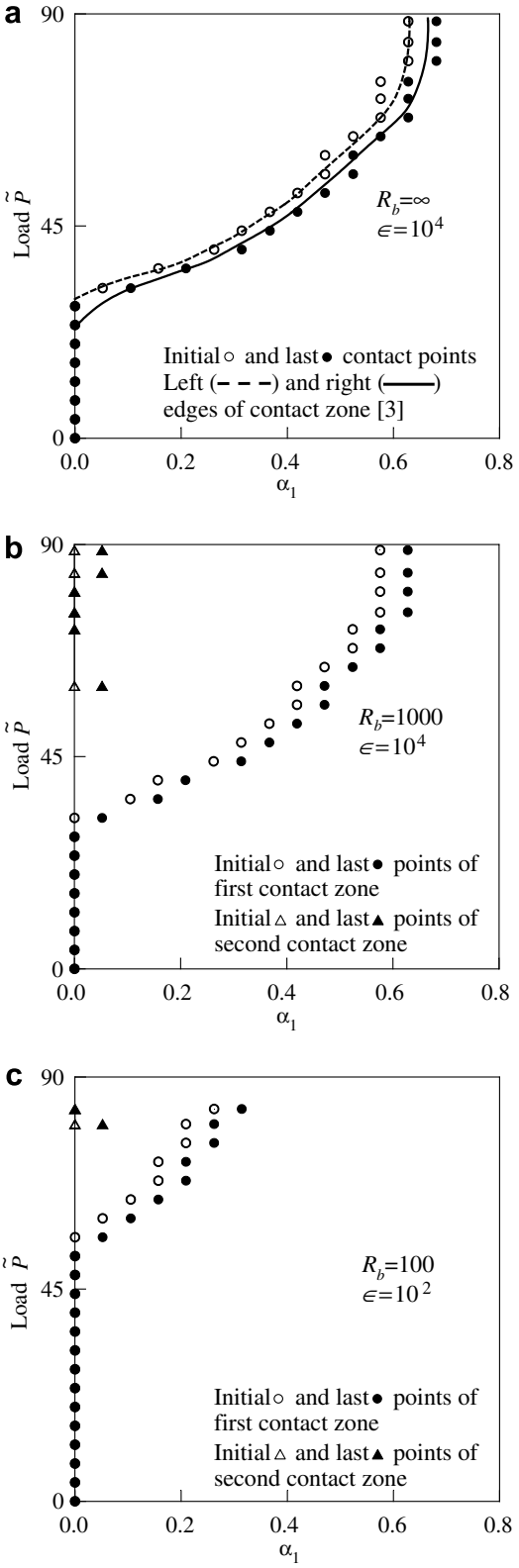

Fig. 9. Circular ring in contact with rigid cylinder. Variation of contact region with loading (modeled by 60×1 mesh) for (a) $R_\mathrm{b}=\infty$, (b) $R_\mathrm{b}=1000$ and (c) $R_\mathrm{b}=100$.

the shell, as in the previous example, is almost inextensional. The geometrical and material characteristics of the

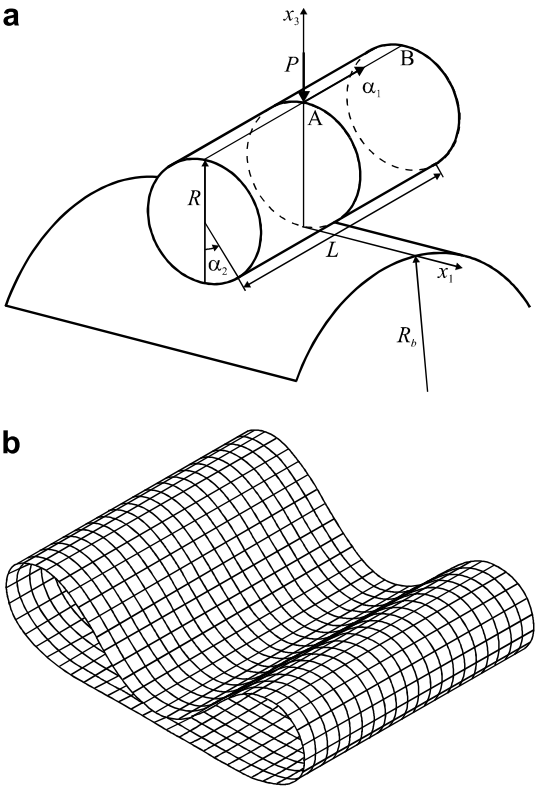

Fig. 10. Cylindrical shell in contact with rigid cylinder: (a) geometry ($E=10^4$, $v=0.3$, $R=100$, $L=200$, $h=1$) and (b) deformed configuration (modeled by 20×60 mesh; $R_\mathrm{b}=1000$, $\widetilde{P}=87.36$, $\epsilon=10^2$).

problem are given in Fig. 10. The impenetrability conditions can be written as

$$\Psi = {}^tR_3 \geqslant 0,$$
$${}^tR_3 = \left(R+\frac{1}{2}h\right)(1-\cos\alpha_2) + v_2^+\sin\alpha_2 - v_3^+\cos\alpha_2 \tag{56a}$$

for a rigid plate and

$$\Psi = \frac{1}{2R_\mathrm{b}}(\alpha_1+v_1^+)^2 + \frac{1}{2R_\mathrm{b}}({}^tR_3+R_\mathrm{b})^2 - \frac{1}{2}R_\mathrm{b} \geqslant 0 \tag{56b}$$

for a rigid cylinder.

Due to symmetry of the problem, only one quarter of the shell is modeled with uniform meshes. Table 5 lists the convergence study for the rigid cylinder of radius $R_\mathrm{b}=1000$. Herein, $\bar{v}_3^\mathrm{A}$ and $\bar{v}_3^\mathrm{B}$ denote the transverse mid-surface displacements at points A and B, whereas $\widetilde{P}=120(1-v^2)PR^2/Eh^3L$ is the dimensionless force and $\widetilde{P}_\mathrm{c}=120(1-v^2)P_\mathrm{c}R^2/Eh^3L$ is the dimensionless contact pressure resultant, where

$$P_\mathrm{c} = 4R\int_0^\pi\int_0^{L/2}\lambda\left(\frac{\partial\Psi}{\partial v_3^+}\cos\alpha_2 - \frac{\partial\Psi}{\partial v_2^+}\sin\alpha_2\right)\mathrm{d}\alpha_1\,\mathrm{d}\alpha_2. \tag{57}$$

As can be seen, in the case of the robust choice of the trial contact zone again only one loading step is required to obtain a converged solution, when a point A practically

Table 5
Convergence study for cylindrical shell subjected to dimensionless load $\widetilde{P} = 87.36$ and interacting with rigid cylinder of radius $R_b = 1000$, where $d_1 = [0,40] \times \{7\pi/30\}$ and $d_2 = \{40\} \times [0,7\pi/30]$

Trial contact zone	Mesh	Penalty parameter $\in$	NLSt	NTESt	NNEt	$\widetilde{P}_c$	$-\bar{v}_3^A$	$-\bar{v}_3^B$
$\{0\} \times \{0\}$[a]	10×30	10^0	3	43	261	87.76	195.0	194.2
$\{0\} \times \{0\}$[a]	10×30	10^2	3	55	314	87.76	195.0	194.2
$\{0\} \times \{0\}$[a]	20×60	10^0	3	39	249	87.46	196.1	195.2
$\{0\} \times \{0\}$[a]	20×60	10^2	3	89	551	87.46	196.1	195.1
$d_1 \cup d_2$	10×30	10^0	1	8	64	87.76	195.0	194.2
$d_1 \cup d_2$	10×30	10^2	1	7	53	87.76	195.0	194.2
$d_1 \cup d_2$	20×60	10^0	1	11	88	87.46	196.1	195.2
$d_1 \cup d_2$	20×60	10^2	1	13	91	87.46	196.1	195.1

[a] Tolerance error is set to be $\varepsilon = 10^{-9}$.

comes into "contact" with the constraint surface. Additionally, Fig. 11 and Table 6 represent load–displacement curves and contact regions for all studied unilateral constraints.

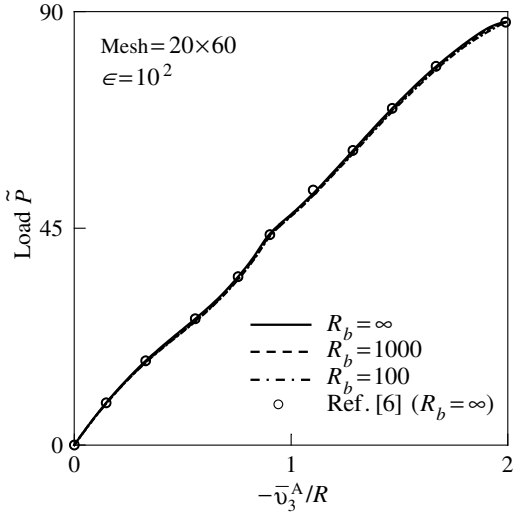

Fig. 11. Cylindrical shell in contact with rigid cylinder. Top load versus transverse displacement of midsurface at section A.

6. Conclusions

The geometrically exact TM shell formulation has been developed for the analysis of thin-walled shell structures undergoing finite deformations and interacting with rigid bodies. The finite element model is based on the perturbed Lagrangian formulation and enhanced finite element technique that a nodal contact force normal to the constraint surface is associated with the Lagrange multiplier λ as $\lambda|\text{grad}\,\Psi|$, where Ψ denotes the impenetrability function. This allows using much larger load increments by employing authors' geometrically exact assumed stress–strain shell formulation compared to conventional isoparametric solid-shell and degenerated-shell formulations with unilateral constraints. It has been shown that in the case of the robust choice of the trial contact zone a solution of the contact problem can be derived in one loading step for the extremely large displacements and rotations.

An important observation is that our element stiffness matrix requires only direct substitutions, i.e., no inversion is needed when sides of the element coincide with the lines of principal curvatures of the reference surface, and it is evaluated, as in Part II, by using the analytical integration. So, the finite element shell formulation developed is very economical and may be used for large scale computations.

Table 6
Cylindrical shell subjected to dimensionless load $\widetilde{P} = 87.36$ and interacting with rigid cylinder (modeled by 20×60 mesh), where $\epsilon = 10^2$, $\alpha_1^a = 15, 20$ and 25, $\alpha_1^b = 55, 60, 65$ and 70, and $\alpha_1^c = 75$ and 80

α_1	Circumferential coordinate α_2																
	0	$\frac{\pi}{60}$	$\frac{2\pi}{60}$	$\frac{3\pi}{60}$	$\frac{4\pi}{60}$	$\frac{5\pi}{60}$	$\frac{6\pi}{60}$	$\frac{7\pi}{60}$	$\frac{8\pi}{60}$	$\frac{9\pi}{60}$	$\frac{10\pi}{60}$	$\frac{11\pi}{60}$	$\frac{12\pi}{60}$	$\frac{13\pi}{60}$	$\frac{14\pi}{60}$	$\frac{15\pi}{60}$	$\frac{16\pi}{60}$
0	⧄	□	□	□	□	□	□	□	□	□	□	□	⧄	⧄	⧄	⧄	□
5	△												○	○	△	△	
10	△												○	○	△		
α_1^a													○	○	△		
30	△	△	△	△									○	⧄	△		
35	⧄	⧄	⧄	△	△	△	△						○	⧄			
40	○	○	○	○	○	○		△	△	△	△		⧄	⧄			
45							○	○				△	○	○			
50									○				○	○			
α_1^b													○	○			
α_1^c														○			

Symbols ○ ($R_b = \infty$), △ ($R_b = 1000$) and □ ($R_b = 100$) exhibit contact nodes.

Acknowledgement

The present research was supported by Russian Fund of Basic Research (Grant No. 07-01-00186).

References

[1] E. Stein, W. Wagner, P. Wriggers, Finite element postbuckling analysis of shells with non-linear contact constraints, in: P.G. Bergan, K.J. Bathe, W. Wunderlich (Eds.), Finite Element Methods for Non-linear Problems, Springer, Berlin, 1986, pp. 719–744.

[2] P. Wriggers, W. Wagner, E. Stein, Algorithms for non-linear contact constraints with application to stability problems of rods and shells, Comput. Mech. 2 (1987) 215–230.

[3] A.K. Noor, K.O. Kim, Mixed finite element formulation for frictionless contact problems, Finite Elements Anal. Des. 4 (1989) 315–332.

[4] J.A. Tanner, V.J. Martinson, M.P. Robinson, Static frictional contact of the space shuttle nose-gear tire, Tire Sci. Technol. 22 (1994) 242–272.

[5] A.K. Noor, J.M. Peters, Reduction technique for tire contact problems, Comput. Struct. 60 (1996) 223–233.

[6] G.M. Kulikov, S.V. Plotnikova, The contact problem for a geometrically non-linear Timoshenko-type shell, J. Appl. Mech. 67 (2003) 825–836.

[7] E.I. Grigolyuk, G.M. Kulikov, S.V. Plotnikova, Contact problem for a pneumatic tire interacting with a rigid foundation, Mech. Compos. Mater. 40 (2004) 427–436.

[8] J.C. Simo, P. Wriggers, R.L. Taylor, A perturbed Lagrangian formulation for the finite element solution of contact problems, Comput. Meth. Appl. Mech. Engrg. 50 (1985) 163–180.

[9] P. Wriggers, J.C. Simo, A note on tangent stiffnesses for fully nonlinear contact problems, Commun. Appl. Numer. Meth. 1 (1985) 199–203.

[10] Z.H. Zhong, Finite Element Procedures for Contact-Impact Problems, Oxford University Press, 1993.

[11] T. Belytschko, W.K. Liu, B. Moran, Nonlinear Finite Elements for Continua and Structures, Wiley, 2000.

[12] G.M. Kulikov, S.V. Plotnikova, Non-linear strain–displacement equations exactly representing large rigid-body motions. Part I. Timoshenko–Mindlin shell theory, Comput. Meth. Appl. Mech. Engrg. 192 (2003) 851–875.

[13] G.M. Kulikov, S.V. Plotnikova, Non-linear strain–displacement equations exactly representing large rigid-body motions. Part II. Enhanced finite element technique, Comput. Meth. Appl. Mech. Engrg. 195 (2006) 2209–2230.

[14] G.M. Kulikov, Analysis of initially stressed multilayered shells, Int. J. Solids Struct. 38 (2001) 4535–4555.

[15] M.F. Ausserer, S.W. Lee, An eighteen-node solid element for thin shell analysis, Int. J. Numer. Meth. Engrg. 26 (1988) 1345–1364.

[16] H.C. Park, C. Cho, S.W. Lee, An efficient assumed strain element model with six dof per node for geometrically nonlinear shells, Int. J. Numer. Meth. Engrg. 38 (1995) 4101–4122.

[17] G.M. Kulikov, S.V. Plotnikova, Equivalent single-layer and layer-wise shell theories and rigid-body motions. Part I: Foundations, Mech. Adv. Mater. Struct. 12 (2005) 275–283.

[18] G.M. Kulikov, S.V. Plotnikova, Equivalent single-layer and layer-wise shell theories and rigid-body motions. Part II: Computational aspects, Mech. Adv. Mater. Struct. 12 (2005) 331–340.

[19] K. Washizu, Variational Methods in Elasticity and Plasticity, Oxford Pergamon Press, 1982.

[20] T.J.R. Hughes, R.L. Taylor, J.L. Sackman, A. Curnier, W. Kanoknukulchai, A finite element method for a class of contact-impact problems, Comput. Meth. Appl. Mech. Engrg. 8 (1976) 249–276.

[21] T.J.R. Hughes, T.E. Tezduyar, Finite elements based upon Mindlin plate theory with particular reference to the four-node bilinear isoparametric element, J. Appl. Mech. 48 (1981) 587–596.

[22] G.M. Kulikov, S.V. Plotnikova, D.V. Kazakov, Contact problem for the elastic plate and rigid body. 1: Geometrically linear formulation, Trans. TSTU 10 (2004) 180–194 (in Russian).

[23] J.C. Simo, P. Wriggers, K.H. Schweizerhof, R.L. Taylor, Finite deformation postbuckling analysis involving inelasticity and contact constraints, in: Proc. Int. Conf. Innovative Methods for Nonlinear Problems, Pineridge Press, Swansea, 1984, pp. 365–387.